ELSEVIER

Comput. Methods Appl. Mech. Engrg. 188 (2000) 269–287

Computer methods in applied mechanics and engineering

www.elsevier.com/locate/cma

On the performance of high aspect ratio elements for incompressible flows

S. Mittal *

Department of Aerospace Engineering, Indian Institute of Technology, Kanpur, UP 208 016, India

Received 1 December 1998

Abstract

A systematic study of the effect of high aspect ratio elements using equal-order-interpolation velocity–pressure elements for computation of incompressible flows is conducted. Both, quadrilateral and triangular elements utilizing, bilinear ($Q1Q1$) and linear ($P1P1$) interpolation functions, respectively, are considered. Stabilized finite-element formulations are employed to solve the incompressible Navier–Stokes equations in the primitive variables. The element length, h, plays an important role in the calculation of stabilizing coefficients in the formulation. Three definitions of h are utilized. These are based on the maximum edge length, minimum edge length of an element and the element length along the streamwise direction. Performance of the implementations is evaluated for both, steady and unsteady flows. Numerical experiments are conducted for flow past a circular cylinder at Reynolds numbers 10 and 100. While in the former case the flow is steady, the latter one is associated with temporally periodic vortex shedding. It is observed that for the $Re = 10$ flow all definitions of h produce acceptable solutions even with elements that have very high aspect ratios. In the case of $Re = 100$ flow, again, all definitions of h work well for elements with reasonable/low aspect ratios. However, for large aspect ratio elements it is only the definition based on the minimum edge length of an element that results in acceptable solution. It is also observed that the effect of high aspect ratio is felt more by the $P1P1$ element as compared to the $Q1Q1$ element.

1. Introduction

Significant progress has been made in the design of stabilized finite element methods since their introduction by Hughes and Brooks [1] as the SUPG (streamline-upwind/Petrov–Galerkin) method for the advection–diffusion equation. It was extended to the solution of Navier–Stokes equations for incompressible flows using $Q1P0$ element (bilinear velocity/constant pressure) by Brooks and Hughes [2]. Later, the method was implemented in the context of multi-step time-integration schemes and with higher order elements by Tezduyar et al. [3]. Hughes et al. [4] proposed a stabilization procedure for Stokes flows that enables one to use elements that do not satisfy the *Brezzi condition.* This was generalized to finite Reynolds number flows by Tezduyar et al. [5]. In this work they proposed the PSPG (pressure-stabilizing/Petrov–Galerkin) stabilizing terms and applied it to the computation of a variety of incompressible flow problems with the equal-order-interpolation velocity–pressure elements. Their work was based on $Q1Q1$ (bilinear velocity/bilinear pressure) and $P1P1$ (linear velocity/linear pressure) elements. A more generalized formulation that is also applicable to higher order interpolations was proposed by Franca et al. [6,7]. This work also includes analysis of the proposed stabilized method for the linearized flow equations. In all the above mentioned efforts, the stabilization terms are element level integrals that are added to the basic Galerkin formulation of the flow equations. They involve certain parameters like the constant C, related to the

* Tel.: +91-512-590151.
E-mail address: smittal@iitk.ac.in (S. Mittal).

0045-7825/00/$ - see front matter
PII: S0045-7825(99)00152-8

bound of error-estimates, and h, the element length, which is an indicator of the mesh size. Several definitions of h have been utilized by various researchers. For regular elements with reasonable aspect ratios they all seem to work well. However, our experience has shown that for elements that are highly stretched in one direction, the correct definition of h becomes an important issue. This is particularly important in the case of high Reynolds number flows, where the gradients in the flow variables normal to the wall are much larger than the ones along the wall and the use of highly stretched elements close to the walls becomes imperative. In such a scenario the correct definition of h is absolutely essential else it may lead to erroneous results. Harari and Hughes [8] carried out a detailed analysis to compute the appropriate values of the constant C and element length h for rectangular and triangular elements that are used in the stabilization terms of the formulation. They worked out the estimates for problems of advection–diffusion, Stokes flows and shear-deformable plates. However, to the best of this authors knowledge, no such estimates are available for computation of unsteady high Reynolds number flows.

In this article a systematic numerical study of the effect of aspect ratio of the elements close to a solid wall is conducted. The stabilized formulation is similar to the one proposed by Tezduyar et al. [5] and by Franca and Frey [7]. Computations are carried out for, both, $Q1Q1$ and $P1P1$ elements. The test problem is the incompressible flow past a circular cylinder at Reynolds number 10 and 100. The $Re = 10$ flow is a steady flow and is fairly close to the Stokes limit and results from Harari and Hughes [8] are expected to hold good. The $Re = 100$ flow is an unsteady flow problem and has been used by various researchers as a benchmark problem (see for example, [5,9–11]). The aspect ratio of the elements close to the cylinder wall is varied from 10 to 10^5 by utilizing different finite element meshes. In all cases, the mesh close to the cylinder differ but remain same far away from it. Three different definitions of h, the element length, are tested. They are based on the maximum edge length, the minimum edge length and the element length along the streamwise direction in an element. To facilitate the comparison of various cases, time-histories of the lift and drag coefficients acting on the cylinder are presented along with the flow pictures and the surface pressure distribution.

The outline of the rest of the article is as follows. We begin by reviewing the governing equations for incompressible fluid flow in Section 2. Section 3 describes the stabilized finite element formulation along with the various definitions of h used in the article. In Section 4 computational results for the test flow problems are presented and discussed followed by a few concluding remarks in Section 5.

2. The governing equations

Let $\Omega \subset \mathbb{R}^{n_{sd}}$ and $(0, T)$ be the spatial and temporal domains, respectively, where n_{sd} is the number of space dimensions, and let Γ denote the boundary of Ω. The spatial and temporal coordinates are denoted by $\mathbf{x}$ and t. The Navier–Stokes equations governing incompressible fluid flow are

$$\rho\left(\frac{\partial \mathbf{u}}{\partial t} + \mathbf{u} \cdot \nabla \mathbf{u} - \mathbf{f}\right) - \nabla \cdot \boldsymbol{\sigma} = 0 \quad \text{on } \Omega \text{ for } (0, T), \tag{1}$$

$$\nabla \cdot \mathbf{u} = 0 \quad \text{on } \Omega \text{ for } (0, T). \tag{2}$$

Here $\rho, \mathbf{u}, \mathbf{f}$ and $\boldsymbol{\sigma}$ are the density, velocity, body force and the stress tensor, respectively. The stress tensor is written as the sum of its isotropic and deviatoric parts:

$$\boldsymbol{\sigma} = -p\mathbf{I} + \mathbf{T}, \quad \mathbf{T} = 2\mu\boldsymbol{\varepsilon}(\mathbf{u}), \quad \boldsymbol{\varepsilon}(\mathbf{u}) = \frac{1}{2}((\nabla \mathbf{u}) + (\nabla \mathbf{u})^{\mathrm{T}}), \tag{3}$$

where p and μ are the pressure and viscosity. Both the Dirichlet and Neumann-type boundary conditions are accounted for, represented as

$$\mathbf{u} = \mathbf{g} \quad \text{on } \Gamma_g, \quad \mathbf{n} \cdot \boldsymbol{\sigma} = \mathbf{h} \quad \text{on } \Gamma_h, \tag{4}$$

where Γ_g and Γ_h are complementary subsets of the boundary Γ. The initial condition on the velocity is specified on Ω:

$$\mathbf{u}(\mathbf{x},0) = \mathbf{u}_0 \quad \text{on } \Omega, \tag{5}$$

where $\mathbf{u}_0$ is divergence free.

3. Finite element formulation

Consider a finite element discretization of Ω into subdomains $\Omega^e, e = 1,2,\ldots,n_{el}$, where n_{el} is the number of elements. Based on this discretization, for velocity and pressure we define the finite element trial function spaces $\mathcal{S}^h_\mathbf{u}$ and $\mathcal{S}^h_p$, and weighting function spaces $\mathcal{V}^h_\mathbf{u}$ and $\mathcal{V}^h_p$. These function spaces are selected, by taking the Dirichlet boundary conditions into account, as subsets of $[\mathbf{H}^{1h}(\Omega)]^{n_{sd}}$ and $\mathbf{H}^{1h}(\Omega)$, where $\mathbf{H}^{1h}(\Omega)$ is the finite-dimensional function space over Ω. The stabilized finite element formulation of Eqs. (1) and (2) is written as follows: find $\mathbf{u}^h \in \mathcal{S}^h_\mathbf{u}$ and $p^h \in \mathcal{S}^h_p$ such that $\forall \mathbf{w}^h \in \mathcal{V}^h_\mathbf{u}$, $q^h \in \mathcal{V}^h_p$

$$\begin{aligned}
&\int \mathbf{w}^h \cdot \rho\left(\frac{\partial \mathbf{u}^h}{\partial t} + \mathbf{u}^h \cdot \nabla \mathbf{u}^h - \mathbf{f}\right) \mathrm{d}\Omega + \int_\Omega \boldsymbol{\varepsilon}(\mathbf{w}^h) : \boldsymbol{\sigma}(p^h,\mathbf{u}^h)\,\mathrm{d}\Omega + \int_\Omega q^h \nabla \cdot \mathbf{u}^h \,\mathrm{d}\Omega \\
&+ \sum_{e=1}^{n_{el}} \int_{\Omega^e} \frac{\tau}{\rho}(\rho \mathbf{u}^h \cdot \nabla \mathbf{w}^h + \nabla q^h) \cdot \left[\rho\left(\frac{\partial \mathbf{u}^h}{\partial t} + \mathbf{u}^h \cdot \nabla \mathbf{u}^h - \mathbf{f}\right) - \nabla \cdot \boldsymbol{\sigma}(p^h,\mathbf{u}^h)\right] \mathrm{d}\Omega^e \\
&+ \sum_{e=1}^{n_{el}} \int_{\Omega^e} \delta \nabla \cdot \mathbf{w}^h \rho \nabla \cdot \mathbf{u}^h \mathrm{d}\Omega^e = \int_\Gamma \mathbf{w}^h \cdot \mathbf{h}^h \,\mathrm{d}\Gamma.
\end{aligned} \tag{6}$$

In the variational formulation given by Eq. (6), the first three terms and the right-hand side constitute the Galerkin formulation of the problem. The terms involving the element-level integrals are the stabilization terms added to the variational formulations [5,6,9] and enable one to use equal-order-interpolation for velocity and pressure. These terms also render stability to the basic Galerkin formulation which is inherently unstable in the presence of the advection operator. The last set of element-level integrals involving δ provide additional stability for flows at large Reynolds numbers. All the stabilization terms are weighted residuals, and therefore maintain the consistency of the formulation. The definitions for τ and δ used in this article are very similar to the ones reported in [5,6,9] and are:

$$\tau(\mathbf{x}) = \left(\left(\frac{2\|\mathbf{u}^h(\mathbf{x})\|}{h}\right)^2 + \left(\frac{8\nu}{m_k h^2}\right)^2\right)^{-1/2}, \tag{7}$$

$$\delta(\mathbf{x}) = \frac{h}{2}\|\mathbf{u}^h(\mathbf{x})\|\xi(Re_u(\mathbf{x})), \tag{8}$$

where

$$m_k = \min\left(\frac{1}{3}, 2C_k\right. \tag{9}$$

$$\xi(Re_u(\;)) = \begin{cases} Re_u(\mathbf{x}) & Re_u(\mathbf{x}) \leqslant \\ 1 & Re_u(\mathbf{x}) > \end{cases} \tag{10}$$

These definitions of the stabilization coefficients are based on their limits for Stokes flow and infinite Reynolds number. C_k is a constant determined from the stability and error analysis and the interested reader is referred to [6,7] for details. For the low order elements like $Q1Q1$ and $P1P1$, used in this article, the value of m_k is $\frac{1}{3}$. For higher order elements, $m_k = \frac{1}{3}$ may lead to oscillatory solution and the correct value must be used [7]. Re_u is the cell Reynolds number and is defined as:

$$Re_u(\mathbf{x}) \tag{11}$$

Three definitions of the element length, h, are utilized

$$h = h_{\min} \equiv \frac{\sqrt{2}A^{e}}{\max(h_{\mathrm{diag}})}$$

$$h = h_{\max} \equiv \frac{\max(h_{\mathrm{diag}})}{\sqrt{2}}$$

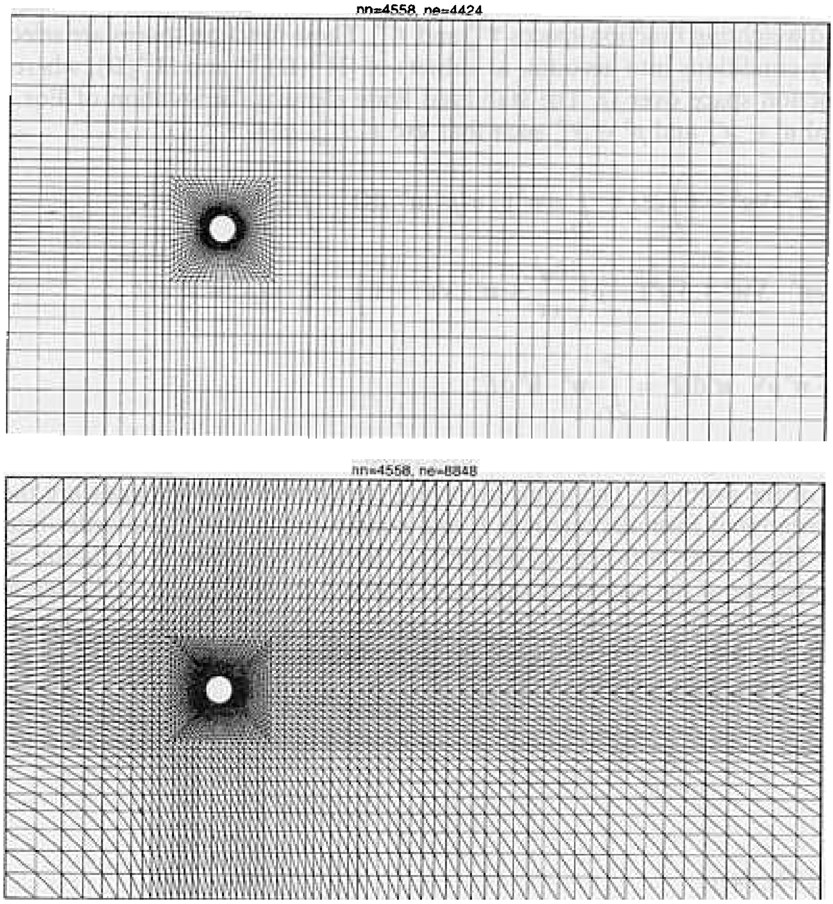

(a)

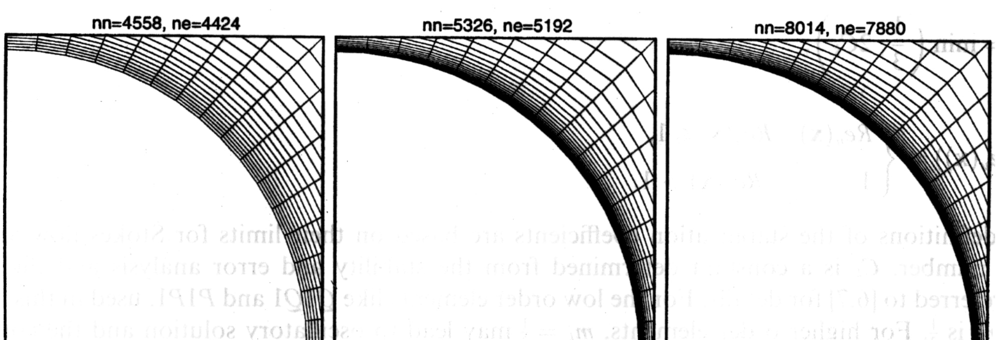

(b)

Fig. 1. Flow past a cylinder: various finite element meshes used in the computations: (a) *Mesh A* and *Mesh* A_t: AR = 10 for elements close to the cylinder. (b) *Mesh A, B and C*: AR = 10, 10^3, 10^5 for elements close to the cylinder.

$$h = h_{\|u\|} \equiv 2\left(\sum_{a=1}^{n_{en}} | \mathbf{s} \cdot \nabla N_a \right) \tag{14}$$

Here, A^e is the area of the element, $\mathbf{s}$ a unit vector in the direction of local velocity, n_{en} the number of local nodes in an element and h_{diag} the length of the diagonal in the case of quadrilateral elements. For triangular elements h_{max} and h_{min} are simply the maximum and minimum edge lengths of the element, respectively. These definitions (and several other variation of these), have been used by researchers in the

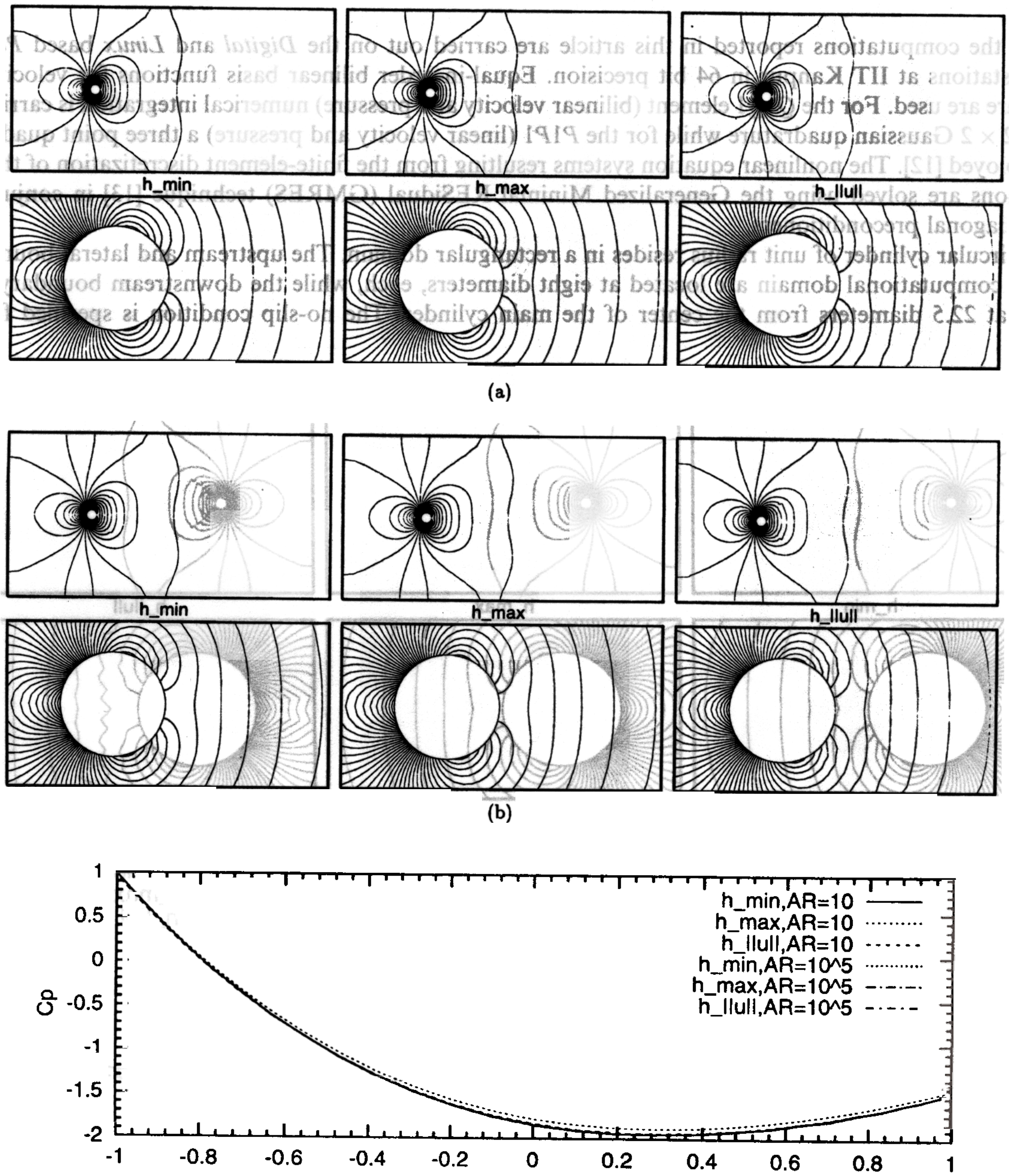

Fig. 2. $Re = 10$ flow past a cylinder computed with $Q1Q1$ element using various definitions of element length: pressure (and its close-up) for the steady-state solution for: (a) AR = 10 (*Mesh A*), and (b) AR = 10^5 (*Mesh C*). Shown in the lower part of the figure is the pressure distribution on the cylinder surface for

past. For example, Tezduyar et al. [5] utilized the definition given by Eq. (14). Harari and Hughes [8] have suggested, for very thin rectangular elements, $h = h_{\min}$ for advection–diffusion equation and a definition of h similar to Eq. (13) for Stokes flows. For highly stretched right triangular elements they suggest $h = \sqrt{2}h_{\min}$ for advection– diffusion equation and $h = \frac{\sqrt{7}}{2}h_{\min}$ for Stokes flows. The time discretization of (6) is done via the generalized trapezoidal rule. For time accurate computations, α is set to 0.5 that results in second-order accuracy in time.

4. Numerical simulations

All the computations reported in this article are carried out on the *Digital* and *Linux* based *Pentium* work-stations at IIT Kanpur in 64 bit precision. Equal-in-order bilinear basis functions for velocity and pressure are used. For the $Q1Q1$ element (bilinear velocity and pressure) numerical integration is carried out via a 2×2 Gaussian quadrature while for the $P1P1$ (linear velocity and pressure) a three point quadrature is employed [12]. The nonlinear equation systems resulting from the finite-element discretization of the flow equations are solved using the Generalized Minimal RESidual (GMRES) technique [13] in conjunction with diagonal preconditioners.

A circular cylinder of unit radius resides in a rectangular domain. The upstream and lateral boundaries of the computational domain are located at eight diameters, each, while the downstream boundary is located at 22.5 diameters from the center of the main cylinder. The no-slip condition is specified for the

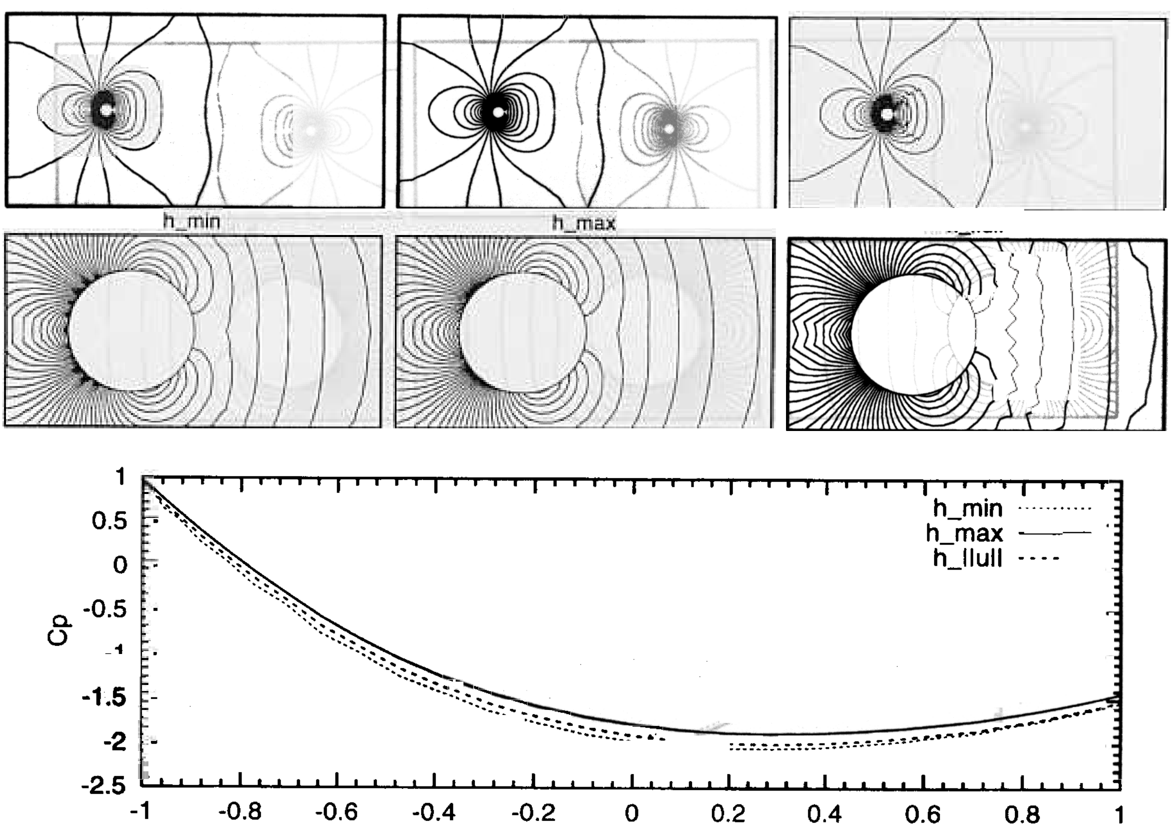

Fig. 3. $Re = 10$ flow past a cylinder computed with $P1P1$ element using various definitions of element length: pressure (and its close-up) for the steady-state solution for *Mesh* B_t with AR $= 10^3$. Shown in the lower part of the figure is the pressure distribution on the cylinder surface for various cases.

velocity on the cylinder wall and free-stream values are assigned for the velocity at the upstream boundary. At the downstream boundary, a Neumann type boundary condition for the velocity that corresponds to zero viscous stress vector is specified. On the upper and lower boundaries, the component of velocity

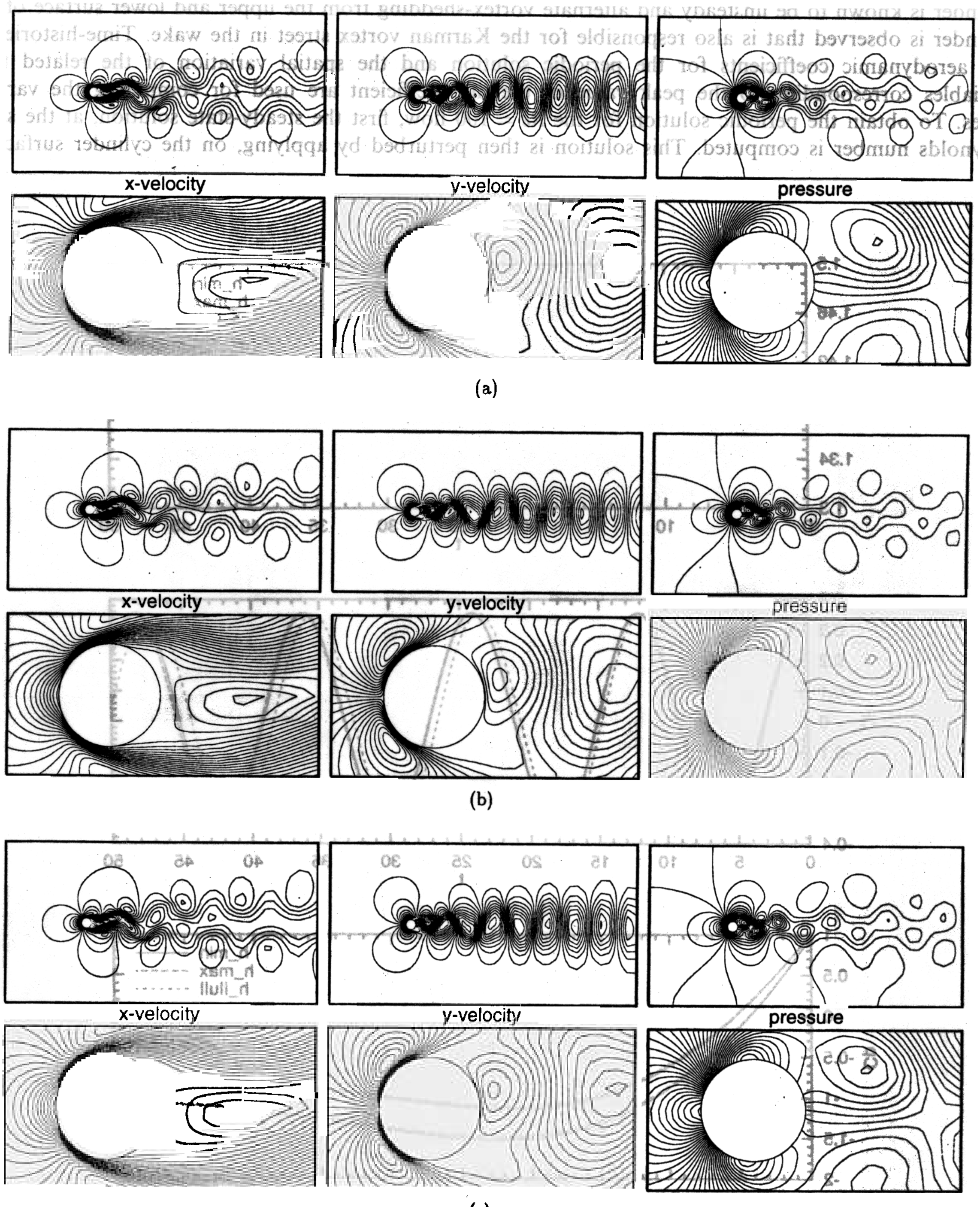

Fig. 4. $Re = 100$ flow past a cylinder computed with $Q1Q1$ element using *Mesh A* (AR = 10 close to the cylinder) and $\Delta t = 0.125$: x-velocity, y-velocity and pressure (and their close-ups) at the peak value of the lift coefficient for the temporally periodic solution for various definitions of element length: (a) $h = h_{\min}$, (b) $h = h_{\max}$ and (c) $h = h_{\|u\|}$.

normal to and the component of stress vector along these boundaries is prescribed zero value. The Reynolds number is based on the diameter of the cylinder, free-stream velocity and the viscosity of the fluid. Computations are carried out for $Re = 10$ and $Re = 100$. At Reynolds number 10 the flow assumes a steady-state and the pressure distribution for the steady-state solution is used as a benchmark to compare the performance of various definitions of h, the element length. $Re = 100$ flow past a circular cylinder is known to be unsteady and alternate vortex-shedding from the upper and lower surface of the cylinder is observed that is also responsible for the Karman vortex street in the wake. Time-histories of the aerodynamic coefficients for the periodic solution and the spatial variation of the related flow variables corresponding to the peak value of the lift coefficient are used for comparing the various cases. To obtain the periodic solution for the $Re = 100$ flow, first the steady-state solution, at the same Reynolds number is computed. This solution is then perturbed by applying, on the cylinder surface, a

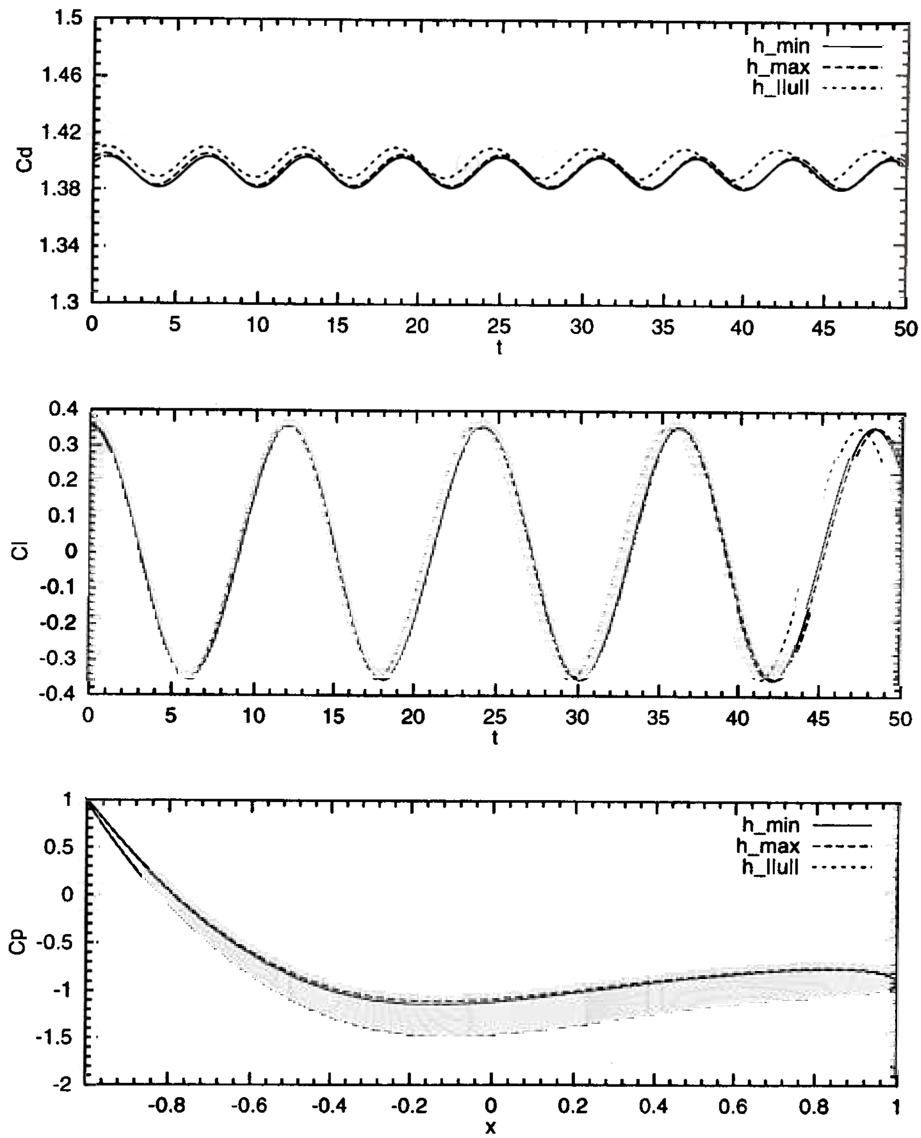

Fig. 5. $Re = 100$ flow past a cylinder computed with $Q1Q1$ element using *Mesh A* (AR = 10 close to the cylinder) and $\Delta t = 0.125$: time-histories of the drag and lift coefficients for the temporally periodic solution and pressure distribution on the cylinder surface corresponding to the peak value of the lift coefficient.

belt-type boundary condition that consists of a set of counter-clockwise and clockwise rotation. Time accurate computations are carried out till a periodic solution develops.

The finite element meshes employed for the computations are designed to adequately resolve the spatial flow structures at Reynolds number 100. To vary the aspect ratio of elements close to the cylinder, number of grid points in the radial direction and their location are varied in a manner that for all cases the mesh far

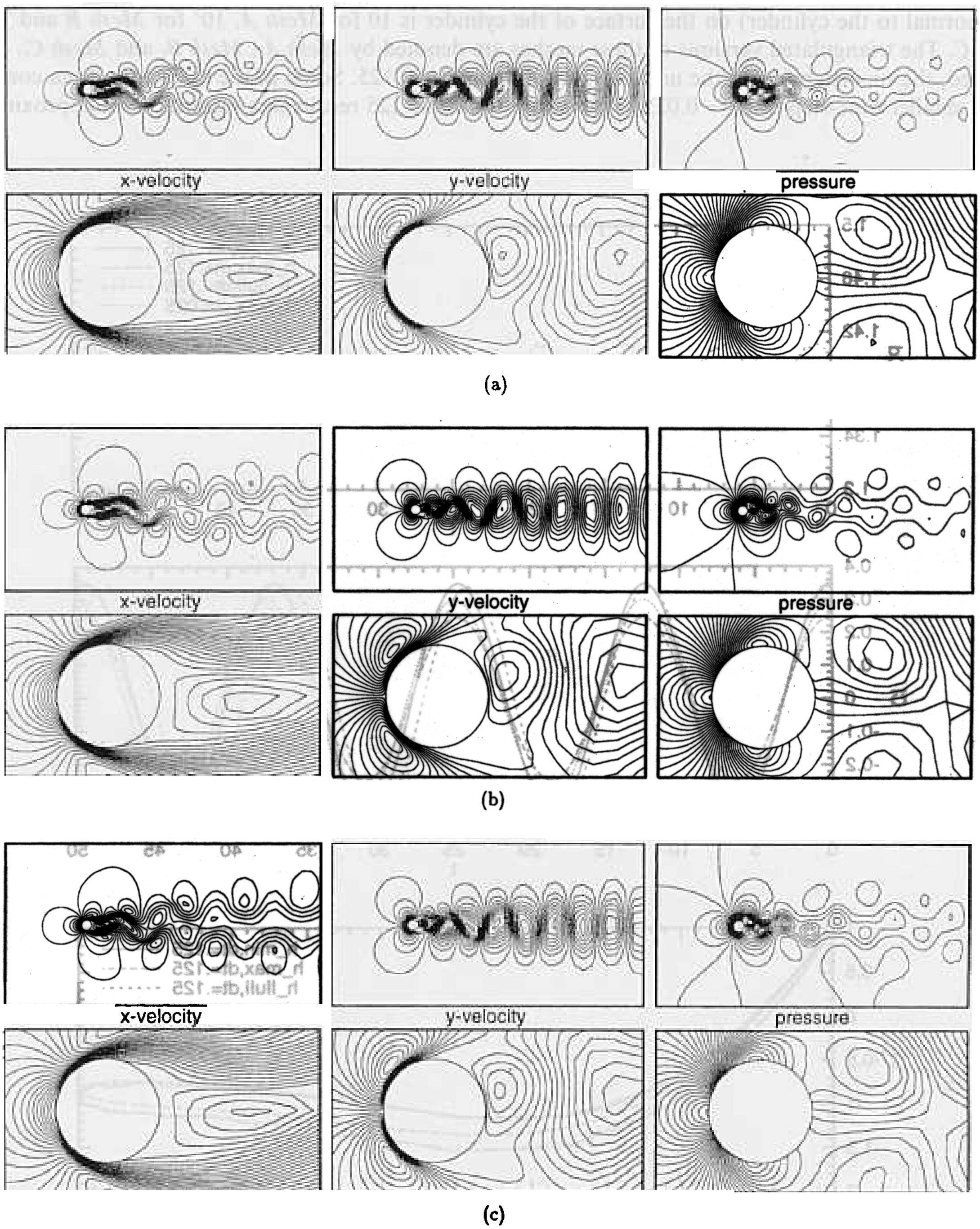

Fig. 6. $Re = 100$ flow past a cylinder computed with $Q1Q1$ element using *MeshB* (AR $= 10^3$ close to the cylinder) and $\Delta t = 0.125$: x-velocity, y-velocity and pressure (and their close-ups) at the peak value of the lift coefficient for the temporally periodic solution for various definitions of element length: (a) $h = h_{\min}$, (b) $h = h_{\max}$ and (c) $h = h_{\|u\|}$.

away from the cylinder remains same. First, the meshes with quadrilateral elements are generated. Meshes with the triangular elements are obtained by simply dividing each quadrilateral into two triangles. Care is taken to preserve the symmetry of the mesh with triangular elements with respect to the x-axis. Fig. 1 shows the various finite element meshes and their close-ups. *Mesh A* consists of 4558 nodes and 4424 quadrilateral elements, *Mesh B* has 5326 nodes and 5192 elements while the numbers for *Mesh C* are 8014 and 7880, respectively. The meshes, in all the cases, outside the small box, enclosing the cylinder (see Fig. 1(a)), are same. The aspect ratio of elements (AR = ratio of the length of edge along the cylinder to the length of the edge normal to the cylinder) on the surface of the cylinder is 10 for *Mesh A*, 10^3 for *Mesh B* and 10^5 for *Mesh C*. The triangulated versions of these meshes are denoted by *Mesh* A_t, *Mesh* B_t and *Mesh* C_t. Unless specified, the time-step for all the unsteady computations is 0.125. Some of the cases have been computed with a smaller time-step of $\Delta t = 0.025$. A time step of $\Delta t = 0.125$ results in a resolution of, approximately,

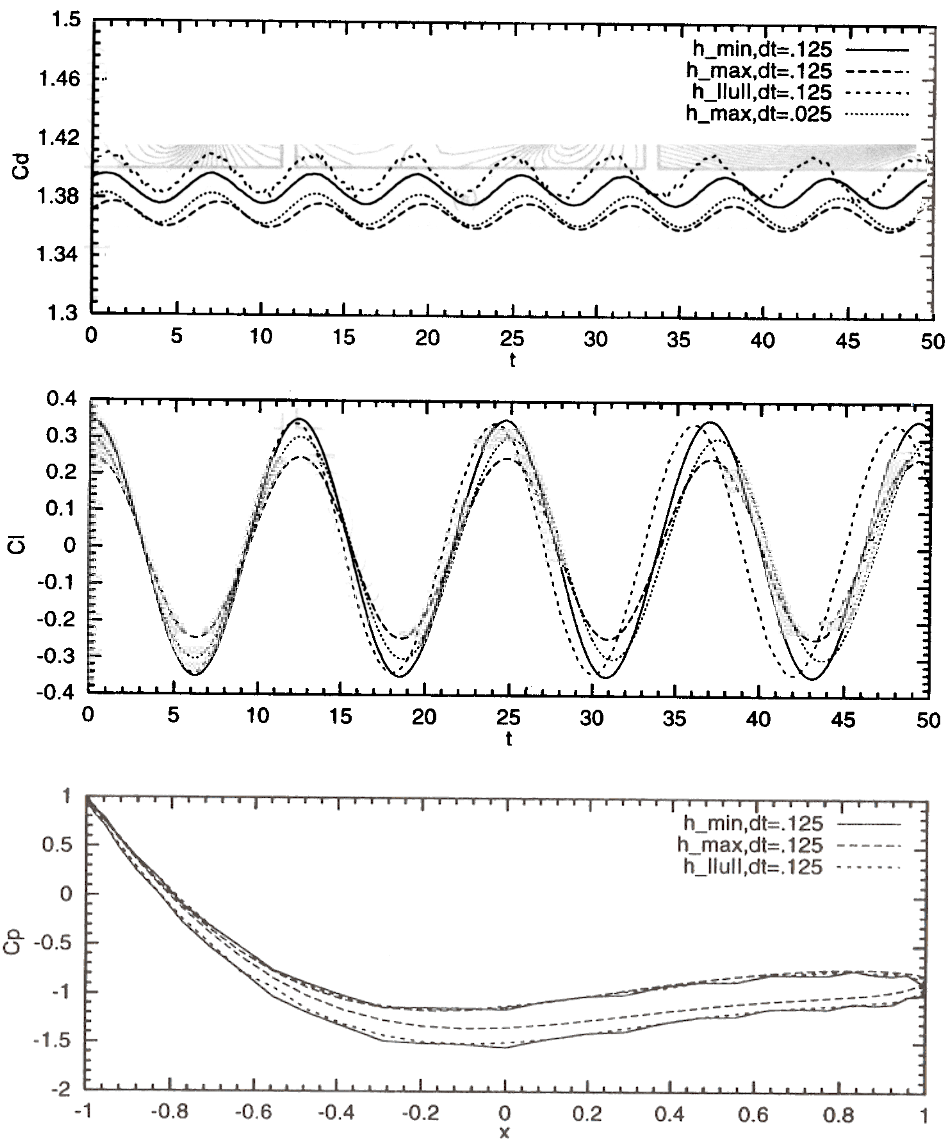

Fig. 7. $Re = 100$ flow past a cylinder computed with $Q1Q1$ element using *MeshB* (AR = 10^3 close to the cylinder): time-histories of the drag and lift coefficients for the temporally periodic solution and pressure distribution on the cylinder surface corresponding to the peak value of the lift coefficient.

100 time-steps per vortex shedding cycle. Our experience has shown this to be sufficient to capture all the details of the flow at this Reynolds number. The pressure coefficient, presented for the various cases, is computed from the pressure field $p(\mathbf{x}, \mathbf{t})$ as $C_p = ((p - p_0)/\frac{1}{2}\rho U_\infty^2) + 1$ where p_0 is the pressure at the leading edge of the cylinder, ρ and U_∞ are the free-stream density and speed, respectively.

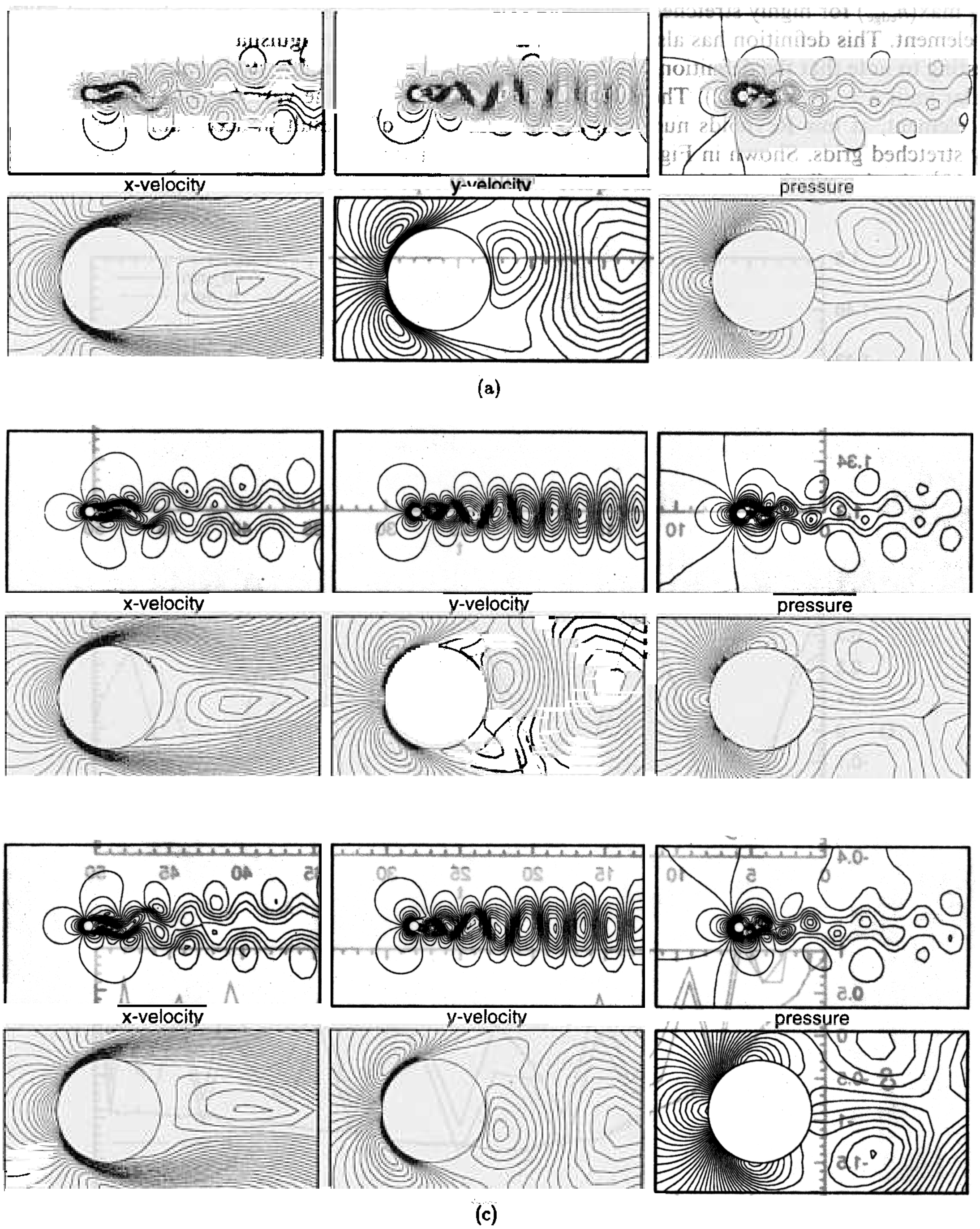

Fig. 8. $Re = 100$ flow past a cylinder computed with $Q1Q1$ element using *Mesh C* (AR $= 10^5$ close to the cylinder) and $\Delta t = 0.125$: x-velocity, y-velocity and pressure (and their close-ups) at the peak value of the lift coefficient for the temporally periodic solution for various definitions of element length: (a) $h = h_{\min}$, (b) $h = h_{\max}$. The time-histories of the force coefficients for case (c) with $h = h_{\|u\|}$ do not exhibit a temporally periodic state.

4.1. $Re = 10$ flow past a cylinder

Fig. 2 shows the steady-state pressure field obtained with the Q1Q1 element for *Mesh A* and *C* and with the three definitions of element length h. It can be observed that all the solutions are quite similar. The C_p distribution for all cases is almost identical except for the one obtained with *Mesh A* and $h = h_{\max}$ which seems to result in a slightly lower value of $| C_p |$. Harari and Hughes [8] have proposed, for Stokes flow, $h = \frac{1}{\sqrt{3}} \max(h_{\text{edge}})$ for highly stretched rectangular elements, where, $\max(h_{\text{edge}})$ is the maximum edge length of an element. This definition has also been used and an almost indistinguishable solution is obtained. It is interesting to note that the definition $h = h_{\max}$ given by Eq. (13), for highly stretched elements, translates to a similar limit $h = \frac{1}{\sqrt{2}} \max(h_{\text{edge}})$. The similarity between results for the various cases suggests that for the $Q1Q1$ element, at low Reynolds numbers, all the definitions of h result in acceptable solutions even for highly stretched grids. Shown in Fig. 3 are the solutions for the $P1P1$ element computed on *Mesh* B_t with $\text{AR} = 10^3$. Again, all the solutions are quite similar except the one with $h = h_{\|u\|}$ which exhibits mild

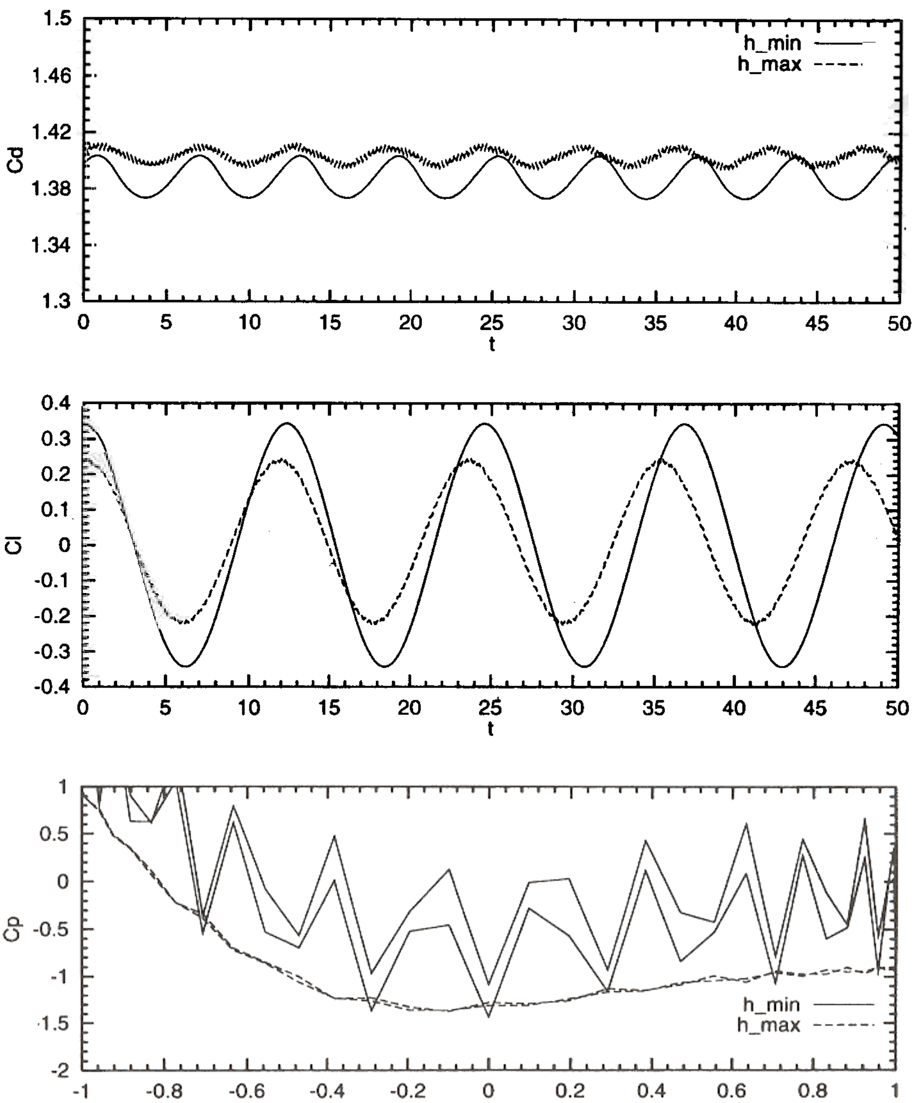

Fig. 9. $Re = 100$ flow past a cylinder computed with $Q1Q1$ element using *Mesh C* ($\text{AR} = 10^5$ close to the cylinder) and $\Delta t = 0.125$: time-histories of the drag and lift coefficients for the temporally periodic solution and pressure distribution on the cylinder surface corresponding to the peak value of the lift coefficient. The case with $h = h_{\|u\|}$ results in large oscillations and is not shown here.

oscillations close to the cylinder. Harari and Hughes [8] have suggested, for Stokes flow, $h = \min(h_{\text{edge}})\sqrt{\frac{7}{4}}$ for highly stretched right triangular elements, where, $\min(h_{\text{edge}})$ is the minimum edge length of an element. This is quite similar to our definition of $h = h_{\min}$ for triangular elements. Computations were also carried out for $Re = 40$ flow and, as expected, a steady-state solution was realized. Similar observations as for $Re = 10$ flow were made. It appears that for low Reynolds number flows, both $h = h_{\min}$ and $h = h_{\max}$ work well.

4.2. *Re = 100 flow past a cylinder*

Flow past a circular cylinder at $Re = 100$ has become a standard benchmark problem and various researchers in the past have reported their computed results which are in good agreement with experimental observations [5,9–11]. It is interesting to note that the results for $Re = 100$ flow past a cylinder presented by Tezduyar et al. [5] were computed on a mesh with AR = 2. Fig. 4 shows the flow pictures for the temporally periodic solution at the peak value of the lift coefficient computed on *Mesh A* (AR = 10) for various definitions of element length. The related time-histories of the aerodynamic coefficients and the C_p distribution on the cylinder surface is shown in Fig. 5. All the different definitions of h result in very similar solutions. Figs. 6 and 7 show the solutions computed on *Mesh B* (AR = 10^3). It can be observed from the time-histories of the aerodynamic coefficients and the C_p distribution in Fig. 7 that, compared to the other cases, $h = h_{\max}$ results in over-diffused solutions. The close-up views of the flow pictures also suggest the same. Interestingly, a lower time-step $\Delta t = 0.025$ improves the solution significantly as can be seen from the plots of the time-histories of the loads. The C_p distribution for $h = h_{\min}$ shows very mild oscillations for this mesh. For the $Q1Q1$ element, the computations on *Mesh C* (AR = 10^5) seem to be the *acid test* for the various definitions of element length. The solutions for this case are shown in Figs. 8 and 9. The definition $h = h_{\max}$ results in overly diffused solution as can be observed from the amplitudes of the unsteady components of load histories and the C_p distribution. Unlike the other definitions, $h = h_{\max}$ results in a solution for which the C_p value from the upper and lower surfaces are very similar. This is perhaps the reason for the low amplitude of the lift coefficient. The definition $h = h_{\|u\|}$ results in very large oscillations in the pressure at the cylinder surface. Consequently, the load histories do not show a temporally periodic nature and exhibit large, very high frequency oscillations. For the same reason, the C_p distribution and the load histories for this case have been omitted in Fig. 9 and the flow pictures corresponding to this case in Fig. 8 are not for the peak value of the lift coefficient but at the end of the computations. It is quite interesting to note that, in some of the cases, despite the local solution being quite inaccurate the far-field solutions, as seen from Fig. 8, are quite similar in all the cases. This may be due to the fact that pressure variation across a boundary layer is quite small and since the numerical oscillations (due to distorted elements) are restricted to a region very close to the cylinder, far away, the flow is almost independent of these oscillations. Perhaps, calculating the loads based on elements that are a few layers farther from the cylinder surface may result in more accurate load histories. Table 1 lists the Strouhal number for the various computations from the different meshes. From the data it can be observed that the definition $h = h_{\min}$ gives nearly the same values for all the three meshes, $h = h_{\max}$ results in a slightly larger value with *Mesh C* while $h = h_{\|u\|}$ breaks down for the mesh with very high aspect ratio elements. All the definitions work fine for elements with reasonable aspect ratios and compare well with results reported by other researchers.

Next, the performance of the $P1P1$ element is evaluated. Figs. 10 and 11 show the solutions obtained with the $P1P1$ element computed on *Mesh* A_t (AR = 10). From the amplitudes of unsteady force coefficients

Table 1
$Re = 100$ flow past a cylinder: Strouhal number for various definitions of h computed on different meshes with the $Q1Q1$ element

Mesh	*nn*	*ne*	AR	*St*		
				$h = h_{\min}$	$h = h_{\max}$	$h = h_{\|u\|}$
Mesh A	4558	4424	10	0.1663	0.1653	0.1691
Mesh B	5326	5192	10^3	0.1626	0.1623	0.1674
Mesh C	8014	7880	10^5	0.1633	0.1709	–

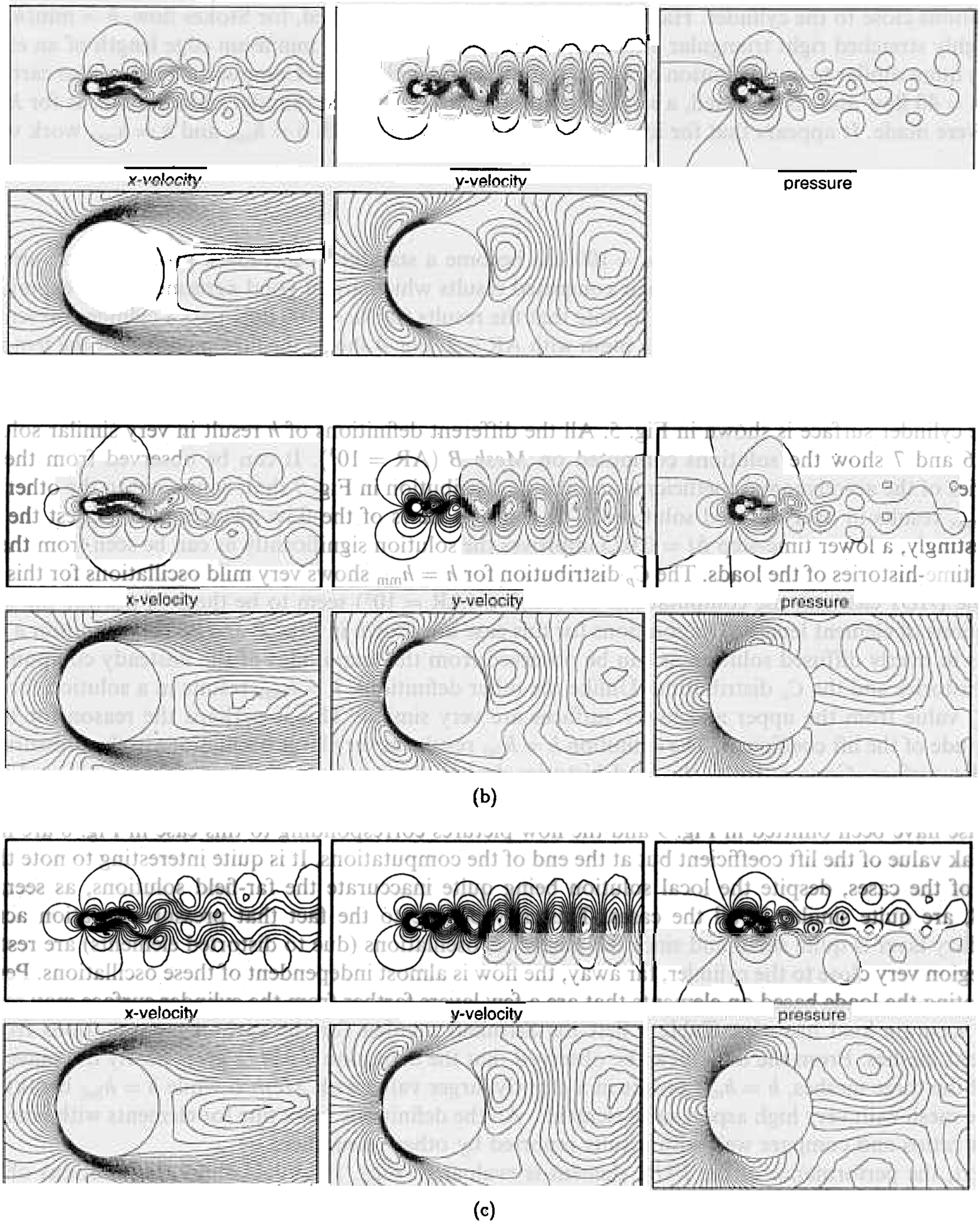

Fig. 10. $Re = 100$ flow past a cylinder computed with $P1P1$ element using $MeshA_t$(AR = 10 close to the cylinder) and $\Delta t = 0.125$: x-velocity, y-velocity and pressure (and their close-ups) at the peak value of the lift coefficient for the temporally periodic solution for various definitions of element length: (a) $h = h_{\min}$, (b) $h = h_{\max}$ and (c) $h = h_{\|u\|}$.

in Fig. 11 it can be observed that the solutions obtained with $h = h_{\max}$ are more diffused compared to the ones obtained with the other two definitions of h. The flow pictures in Fig. 10 also suggest the same. It can be observed, from Fig. 11, that the effect of the time-step is quite insignificant. This is in sharp contrast to the observation made for the $Q1Q1$ element where a reduction in the time-step leads to lesser numerical diffusion. The solutions for higher aspect ratio elements (AR $= 10^3$) computed on $Mesh\ B_t$ are shown in

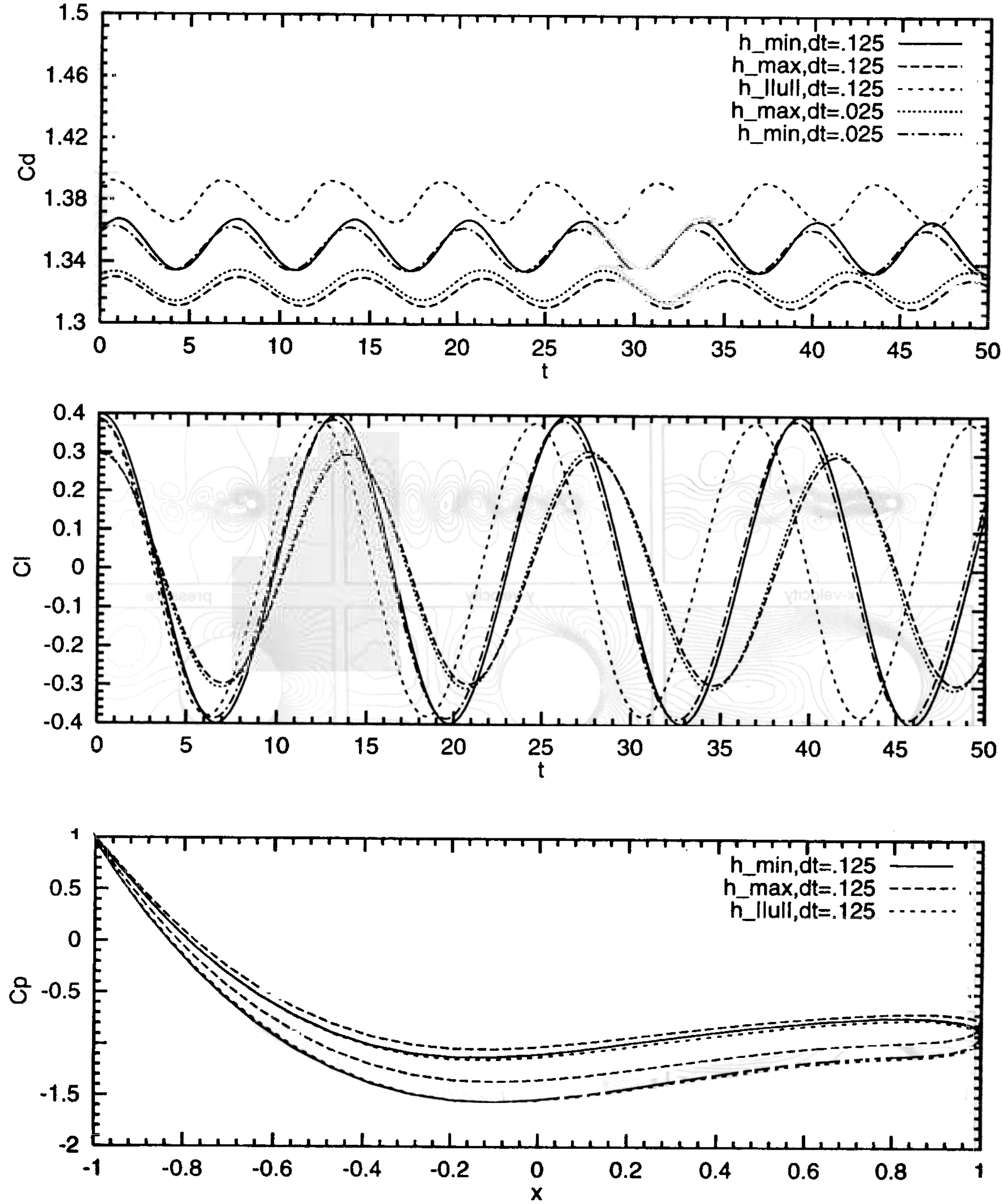

Fig. 11. $Re = 100$ flow past a cylinder computed with $P1P1$ element using $Mesh A_t$(AR = 10 close to the cylinder): time-histories of the drag and lift coefficients for the temporally periodic solution and pressure distribution on the cylinder surface corresponding to the peak value of the lift coefficient.

Figs. 12 and 13. With $h = h_{\max}$ the solution close to the cylinder is overly diffused as can be seen from the flow pictures and time-histories of the force coefficients. The C_p values at the lower and upper surface of the cylinder, at any x location, are same. The definition $h = h_{\|u\|}$ results in oscillatory solutions as can be noticed in the C_p and time-histories plots. However, $h = h_{\min}$ results in quite acceptable solution. As observed with $Mesh\, A_t$, the reduction in time-step does not seem to affect the solution significantly. It appears

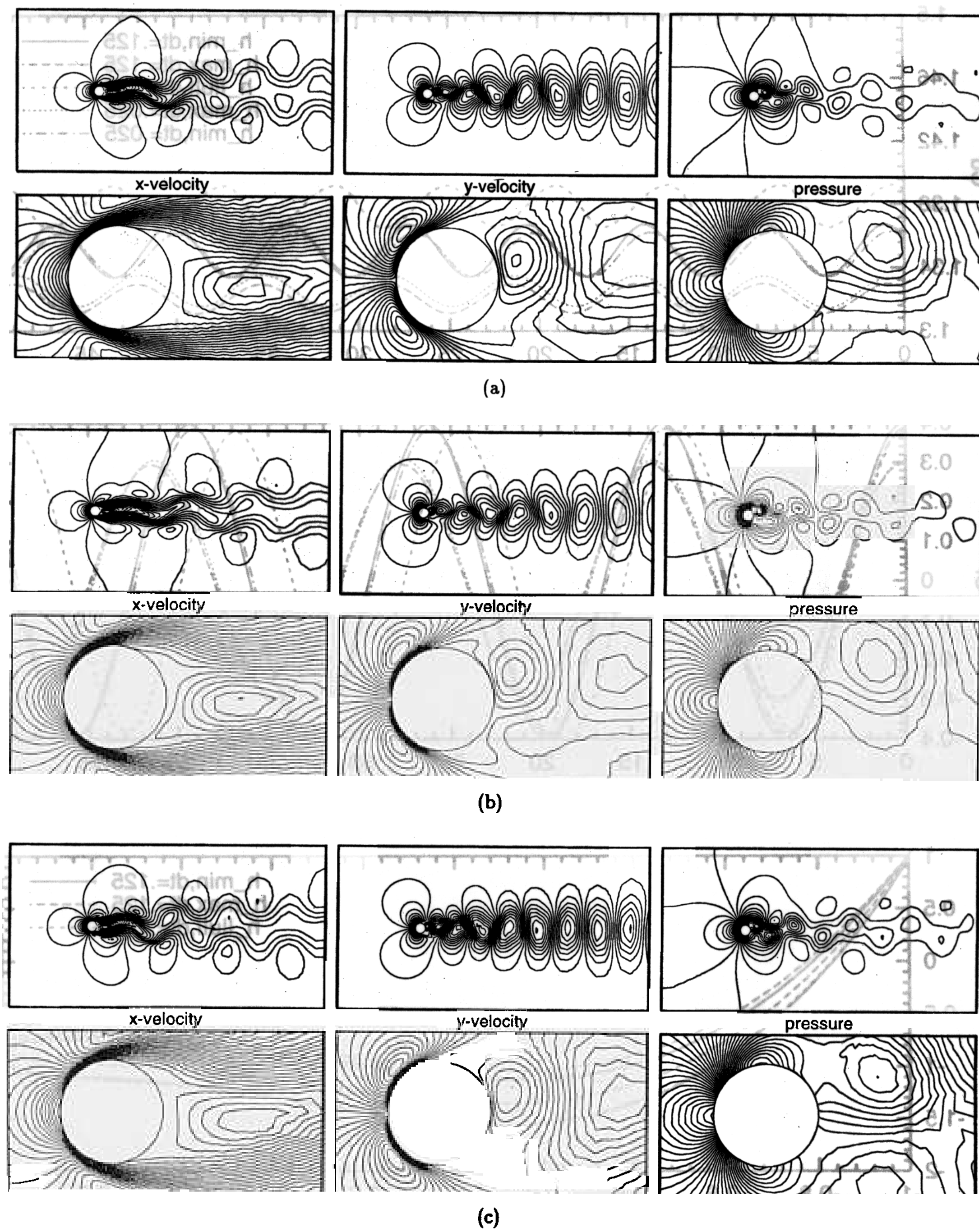

Fig. 12. $Re = 100$ flow past a cylinder computed with $P1P1$ element using $MeshB_t$(AR $= 10^3$ close to the cylinder) and $\Delta t = 0.125$: x-velocity, y-velocity and pressure (and their close-ups) at the peak value of the lift coefficient for the temporally periodic solution for various definitions of element length: (a) $h = h_{\min}$, (b) $h = h_{\max}$ and (c) $h = h_{\|u\|}$.

that the definition $h = h_{\min}$ performs the best amongst the three definitions that have been evaluated in this article. Table 2 lists the Strouhal number for the various computations with the $P1P1$ element.

From the data it can be observed that all definitions of h result in lower values of St as the AR increases and that compared to the other two definitions, $h = h_{\max}$ consistently results in smaller values. In general, the value of St obtained from $P1P1$ element is smaller than the corresponding value obtained from the

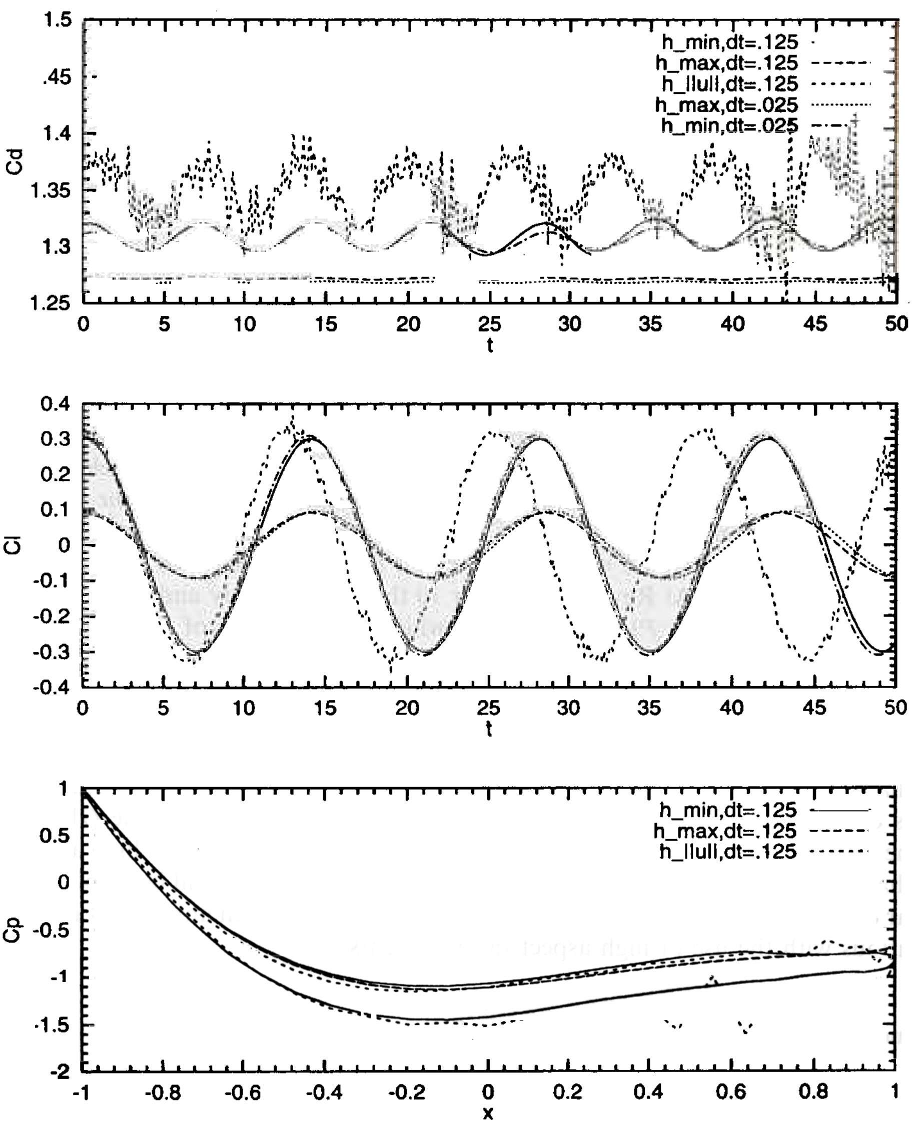

Fig. 13. $Re = 100$ flow past a cylinder computed with $P1P1$ element using *MeshB*$_t$ (AR $= 10^3$ close to the cylinder): time-histories of the drag and lift coefficients for the temporally periodic solution and pressure distribution on the cylinder surface corresponding to the peak value of the lift coefficient.

Table 2
$Re = 100$ flow past a cylinder: Strouhal number for various definitions of h computed on different meshes with the $P1P1$ element. The values without parentheses are the ones obtained with $\Delta t = 0.125$ while the ones in the parentheses have been computed with $\Delta t = 0.025$

Mesh	*nn*	*ne*	AR	*St*		
				$h = h_{min}$	$h = h_{max}$	$h = h_{\|u\|}$
Mesh A_t	4558	8848	10	0.1530 (0.1533)	0.1449 (0.1452)	0.1633
Mesh B_t	5326	10384	10^3	0.1429 (0.1432)	0.1396 (0.1383)	0.1536
Mesh D_t	5742	11088		0.1610	0.1521	0.1667

$Q1Q1$ element. Also, the $Q1Q1$ element works fine with all definitions of h for a mesh with AR $= 10^3$ while some definitions cease to provide acceptable solution for the mesh with AR $= 10^5$. For the $P1P1$ element, even for meshes with AR $= 10^3$, some definitions of h do not work satisfactorily. This suggests that the $Q1Q1$ element is more forgiving than the $P1P1$ element with respect to its ability to produce acceptable results with highly stretched elements. As expected, the computations reported by Tezduyar et al. [5], that have been carried out using a mesh with 5350 nodes and AR = 2 close to the cylinder and with the definition of h as $h = h_{\|u\|}$, compare quite well with the results in the present article using the *Mesh A* and *Mesh* D_t.

5. Concluding remarks

High aspect ratio elements are often needed in computation of flows, especially at high Reynolds numbers. A systematic computational study to investigate the effect of high aspect ratio elements on computation of incompressible flows using equal-order-interpolation for velocity–pressure has been conducted. Quadrilateral elements with bilinear interpolation ($Q1Q1$) and triangular elements with linear interpolation functions ($P1P1$) have been considered. Three definitions of the *element length* (h) are utilized. These are based on the maximum edge length of an element, minimum edge length of an element and the element length along the stream-wise direction. The test problem is the flow past a circular cylinder at Reynolds numbers 10 and 100. At Reynolds number 10 the flow is steady and all definitions of h result in acceptable solution except for the $P1P1$ element for which the definition of h based on the magnitude of velocity results in mild oscillations with a mesh having elements of AR $= 10^3$ close to the cylinder. For the $Re = 100$ flow it is observed that $h = h_{\min}$ performs the best. Even for mesh with very large aspect ratio elements close to the cylinder, acceptable solutions are obtained with this definition. The definition based on maximum edge length results in overly diffused solution while the one based on velocity-magnitude produces oscillatory solutions close to the cylinder. However, for elements with reasonable aspect ratios, all the definitions of h seem to produce acceptable solutions. It is observed that the $Q1Q1$ element is more robust than the $P1P1$ element in the sense of providing acceptable solutions with high aspect ratio elements. It is also felt that a re-look at the definition of the stabilizing coefficient, τ, will be helpful. Perhaps, τ should be a non-scalar quantity and should incorporate the stretching of grids. In any case, it is advocated that one should be cautious with the use of high aspect ratio elements.

Acknowledgements

The author is grateful to Prof. C.S. Upadhyay, Department of Aerospace Engineering, IIT Kanpur, for his participation in the discussions with the author and for his suggestions during this work.

References

[1] T.J.R. Hughes, A.N. Brooks, A multi-dimensional upwind scheme with no crosswind diffusion, in: T.J.R. Hughes (Ed.), Finite Element Methods for Convection Dominated Flows, AMD-vol. 34, ASME, New York, 1979, pp. 19–35.
[2] A.N. Brooks, T.J.R. Hughes, Streamline upwind/Petrov–Galerkin formulations for convection dominated flows with particular emphasis on the incompressible Navier–Stokes equations, Computer Methods in Applied Mechanics and Engineering 32 (1982) 199–259.
[3] T.E. Tezduyar, Stabilized finite element formulations for incompressible flow computations, Advances in Applied Mechanics 28 (1991) 1–44.
[4] T.J.R. Hughes, L.P. Franca, M. Balestra, A new finite element formulation for computational fluid dynamics: V. Circumventing the Babuška–Brezzi condition: A stable Petrov–Galerkin formulation of the Stokes problem accommodating equal-order interpolations, Computer Methods in Applied Mechanics and Engineering 59 (1986) 85–99.
[5] T.E. Tezduyar, S. Mittal, S.E. Ray, R. Shih, Incompressible flow computations with stabilized bilinear and linear equal-order-interpolation velocity–pressure elements, Computer Methods in Applied Mechanics and Engineering 95 (1992) 221–242.
[6] L.P. Franca, S.L. Frey, T.J.R. Hughes, Stabilized finite element methods: I. Application to the advective–diffusive model, Computer Methods in Applied Mechanics and Engineering 95 (1992) 253–276.
[7] L.P. Franca, S.L. Frey, Stabilized finite element methods: II. The incompressible Navier–Stokes equations, Computer Methods in Applied Mechanics and Engineering 99 (1992) 209–233.

[8] I. Harari, T.J.R. Hughes, What are c and h?: Inequalities for the analysis and design of finite element methods, Computer Methods in Applied Mechanics and Engineering 97 (1992) 157–192.
[9] S. Mittal, Stabilized Space-time finite element formulations for unsteady incompressible flows involving fluid-body interactions, Ph.D. Thesis, University of Minnesota (1992).
[10] M. Behr, J. Liou, R. Shih, T.E. Tezduyar, Vorticity-stream function formulation of unsteady incompressible flow past a cylinder: Sensitivity of the computed flow field to the location of the outflow boundary, International Journal of Numerical Methods in Fluids 12 (1991) 323–342.
[11] M. Behr, D. Hastreiter, S. Mittal, T.E. Tezduyar, Incompressible flow past a circular cylinder: Dependence of the computed flow field on the location of the lateral boundaries, Computer Methods in Applied Mechanics and Engineering 123 (1995) 309–316.
[12] T.J.R. Hughes, The Finite Element Method, Linear Static and Dynamic Finite Element Analysis, Prentice-Hall, Englewood Cliffs, NJ, 1987.
[13] Y. Saad, M. Schultz, GMRES: A generalized minimal residual algorithm for solving nonsymmetric linear systems, SIAM Journal of Scientific and Statistical Computing 7 (1986) 856–869.